SEPTEMBER 2009 | VOLUME III | ISSUE VIII

Qpedia

IN THIS ISSUE

Qpedia

SUBSCRIBE ON LINE AT:
www.qats.com/qpedia

Advanced Thermal Solutions is a leading engineering and manufacturing company supplying complete thermal and mechanical packaging solutions from analysis and testing to final production. ATS provides a wide range of air and liquid cooling solutions, laboratory-quality thermal instrumentation, along with thermal design consulting services and training. Each article within Qpedia is meticulously researched and written by ATS' engineering staff and contributing partners. For more information about Advanced Thermal Solutions, Inc., please visit www.qats.com or call 781-769-2800.

EDITOR
KAVEH AZAR, Ph.D.
President & CEO,
Advanced Thermal Solutions, Inc.

MANAGING EDITOR
BAHMAN TAVASSOLI, Ph.D.
Chief Technology Officer,
Advanced Thermal Solutions, Inc.

NORTH AMERICA
ADVANCED THERMAL SOLUTIONS, INC.
89-27 Access Road Norwood, MA 02062 USA
T: 781.769.2800 | F: 781.769.9979 | www.qats.com

EUROPE
ADVANCED THERMAL SOLUTIONS, B.V.
De Nieuwe Vaart 50 | 1401 GS Bussum
The Netherlands
T: +31 (0) 3569 84715 | F: +31 (0) 3569 21294
www.qats-europe.com

ADVERTISING
TO PLACE AN AD IN QPEDIA:

Contact Ray Santos at 781.769.2800

Qpedia was launched in 2007 as a technology eMagazine focused on the thermal management of electronics. It is designed as a resource to help the engineering community solve the most challenging thermal problems.

The eMagazine is published monthly and distributed at no charge to over 21,000 engineers worldwide. Qpedia is also available online or for download at www.qats.com/qpedia.

Qpedia's editorial team includes ATS' President & CEO, Kaveh Azar, Ph.D., and Bahman Tavassoli, Ph.D., the company's chief technologist. Both Azar and Tavassoli are internationally recognized experts in the thermal management of electronics.

For more information on how you can generate awareness about your company or products, contact Ray Santos at 781.769.2800.

Qpedia

Features


Heat issues have you tangled up?
LET THE EXPERTS AT ATS SHOW YOU HOW TO ENSURE PRODUCT RELIABILITY, SPEED TIME-TO-MARKET AND REDUCE COSTS WITH EXPERT THERMAL MANAGEMENT ANALYSIS AND DESIGN SERVICES.

LED Lighting: A Case Study

in Thermal Management

This article examines the thermal management of a light emitting diode (LED)-based lighting system. First, we discuss the environment in which the lighting system will be used. Then, we look at the system's cooling needs and the various analyses used to confirm that the LED thermal requirements are being met. The article concludes with a comparison of the results.

LED-Based Lighting System Requirements

An LED-based lighting system was to be designed to replace a halogen-based downlight. A downlight is typically installed in a hollow opening in a ceiling and provides a concentrated output in the downward direction. A thermal management analysis was needed to properly design a cooling method for the LED system, which had to include a natural convection heat sink. This environment is shown in Figure 1

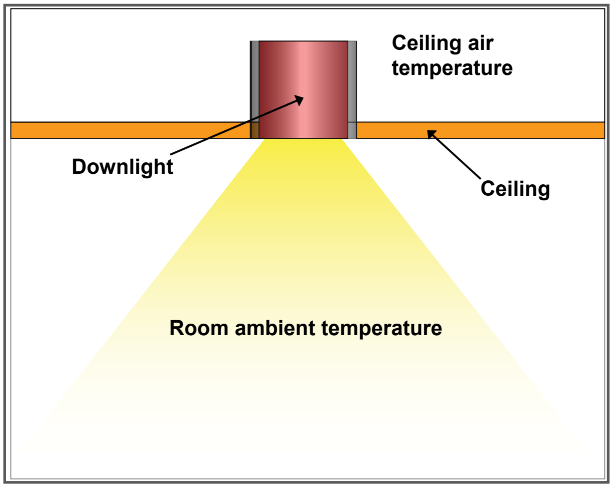

Figure 1. A Typical Downlight Environment.

Product Requirements

The lifetime of an LED relates to its junction temperature and forward current. The new downlight includes three InGaN-based LUXEON cool white K2 LEDs at a forward current of 1000 mA. The maximum operational junction temperature for these cool white LEDs is 150ºC [1]. The downlight has a lifetime requirement of 60,000 hours. Figure 2 shows the lifetimes of the cool white LED for different forward currents, junction temperatures, and for the B10, L70 lifetime condition (which implies that for a specific lifetime, 10% of the LEDs are expected to fail at the specified junction temperature and forward current.) The failure criterion is when the light output of the LED has been reduced to 70% of its original light out. To achieve the 60,000 hours lifetime with a B10, L70 condition, the junction temperatures required for specific forward currents are shown in Table 1. From Table 1, with a forward current of 1000 mA, the junction temperature needs to be kept below 124ºC to achieve a 60,000 hours lifetime.

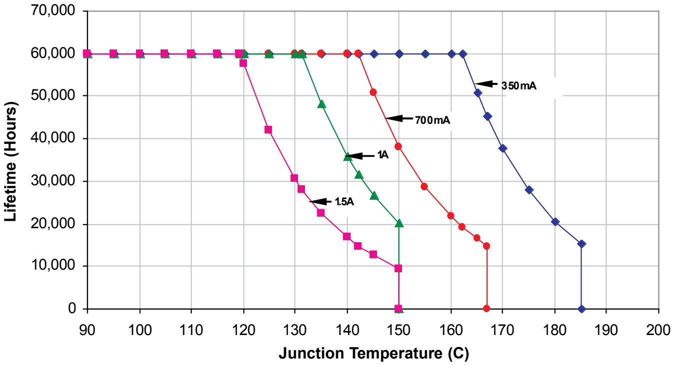

Figure 2. Lifetimes for Different InGaN Versions of the LUXEON K2 LED [2].

Table 1. Required Junction Temperatures of LUXEON K2 LEDs for Specific Forward Currents to Achieve 60,000 Hours Lifetime Under the B10, L70 Lifetime Condition [2].

Forward Current [mA]	Max Junction Temperature [ºC]
350	154
700	134
1000	124
1500	112

For this study, in order to achieve a 60,000 hours lifetime the LED junction temperature must be kept under 124ºC, with an average year-round temperature of 20ºC. Under maximum temperature conditions, the junction temperature must be less than 150ºC at an ambient temperature of 40ºC.

Thermal Management Analysis

The lifetime and maximum temperature conditions were determined previously; now, a thermal management analysis is applied to each condition. This is a confidence level analysis performed to build in safety margins for all unknowns in all engineering phases. The analysis comprises three sections: analytical, numerical (CFD) and experimental.

1. Analytical analysis
    a. Based on the unknowns in the analysis and shortcomings of empirical and experimental correlations, assumptions made in order to do the analysis
2. Numerical or CFD analysis
    a. Unknowns and assumptions made in order to do the analysis
    b. Shortcomings in the numerical code
3. Experimental
    a. Incorrect thermocouple placement
    b. Variations in thermocouple response
    c. Errors in velocity probe calibration
    d. Power input measurement

Equation 1 is used for the confidence level analysis, where T_j is the required junction temperature and *CFL* is the confidence level being applied. Additionally, $T_{j,condiction}$ is the specified junction temperature and $T_{reference}$ is the reference or ambient temperature. The temperature difference between the required junction temperature and the reference temperature, $\Delta T_{condition}$, is used when comparing different conditions.

$$\frac{T_j - T_{reference}}{T_{j,condition} - T_{reference}} = \frac{\Delta T_{condition}}{T_{j,condition} - T_{reference}} \leq CFL \quad (1)$$

Table 2. Confidence Factor Level, CFL, for Different Types of Analyses.

Type of Analysis	CFL
Analytical	80%
Numerical	80% to 85%
Experimental	90%

A confidence level of 90% is used in this study. Re-arranging Equation 1 yields Equation 2. Applying the lifetime conditions to Equation 2 determines the temperature difference for the lifetime condition.

$$\Delta T_{condition} = CFL \times \left(T_{j,condition} - T_{reference}\right) \quad (2)$$

$$\Delta T_{lifetime} = 0.9 \times (124 - 20) = 93.6\ K \quad (3)$$

The maximum temperature difference can also be determined, as shown in Equation 4.

$$\Delta T_{maximum} = 0.9 \times (150 - 40) = 99\ K \quad (4)$$

From Equations 3 and 4, the lifetime condition is the most severe condition. Re-arranging Equation 1 yields Equation 5, which, applied to the lifetime condition, gives us Equation 6.

$$T_j = CFL \times \left(T_{j,condition} - T_{reference}\right) + T_{reference} \quad (5)$$

Thermal Management Design Kit

ATS-TMDK-96

ATS ADVANCED THERMAL SOLUTIONS, INC.
Innovations in Thermal Management®

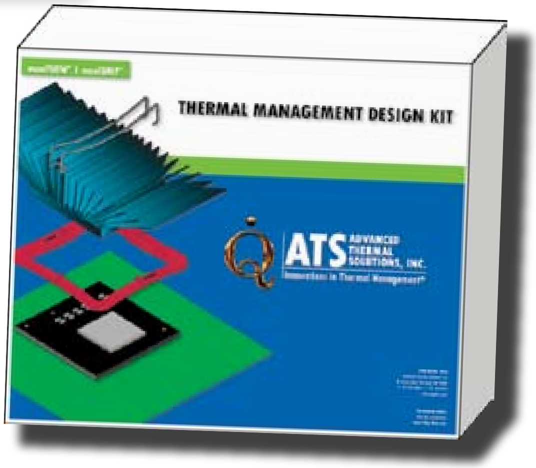

Advanced Thermal Solutions' Thermal Management Design Kit contains 96 of its best-selling maxiFLOW™ heat sinks and maxiGRIP™ sink attachment systems, to quickly provide optimum component cooling solutions during the prototyping, trouble shooting and final design stages.

There are 288 parts in all, including heat sink, frame clip, spring clip and pre-applied thermal interface material for 16 of the most common component sizes available. This allows engineers to have the best cooling solution available for nearly every application.

ATS maxiFLOW heat sinks feature a low profile, spread fin array to maximize surface area for more effective air (convective) cooling. The maxiGRIP heat sink attachment system features a plastic frame clip and a stainless steel spring clip that runs through the heat sink's fin field, fastens securely to the plastic frame and applies steady, even pressure to the component throughout the product lifecycle.

Every heat sink in the Kit comes with a high quality thermal interface material to enhance cooling performance and allow immediate qualification testing. An enclosed catalog provides each heat sink's part number, dimensions (base and fin tip to fin tip) and cooling performance in both ducted and unducted airflow conditions.

All parts in the kit are RoHS compliant.

Individual orders of maxiFLOW heat sinks with maxiGRIP frame and spring clip assemblies, including replacements for the Kits, are available exclusively from Digi-Key, and can be ordered at digikey.com. Tools that aid in the installation and removal of the assemblies are also available and can be ordered from Digi-Key or ATS.

COMPONENT SIZES:

17 mm x 17 mm
19 mm x 19 mm
21 mm x 21 mm
23 mm x 23 mm
25 mm x 25 mm
27 mm x 27 mm
29 mm x 29 mm
30 mm x 30 mm
31 mm x 31 mm
32.5 mm x 32.5 mm
33 mm x 33 mm
35 mm x 35 mm
37.5 mm 37.5 mm
40 mm x 40 mm
42.5 mm x 42.5 mm
45 mm x 45 mm

COMPONENT HEIGHTS:

Standard - 3 mm to 4.5 mm
Low Profile - 1.5 mm to 2.99 mm

HEAT SINK HEIGHTS:

STD	LP
7.5 mm	9.5 mm
12.5 mm	14.5 mm
17.5 mm	19.5 mm

» **96 Heat Sink Assemblies**
Each includes a heat sink, with pre-applied phase-changing thermal interface material, plastic frame clip and stainless steel spring clip

» **Ideal for Prototyping & Testing**
Allows engineers to have the best cooling solution available for nearly every application

» **Parts Available from Digi-Key**
Additional samples and replacement parts are conveniently available from Digi-Key and can be ordered at www.digikey.com

» **maxiFLOW™ Heat Sinks**
maxiFLOW heat sinks reduce device junction temperatures (T_J) by more than 20 percent, compared with other heat sinks of comparable volume

» **maxiGRIP™ Attachment**
Provides secure heat sink attachment and applies steady, even pressure to the component throughout the product lifecyle

» **Meets Shock & Vibration Standards**
maxiGRIP assemblies are certified to meet Telcordia, ETSI and MIL-STD vibration and shock test standards

» **Detailed Performance Data**
An enclosed catalog provides each heat sink's part number, dimensions (base and fin tip to fin tip) and cooling performance in both ducted and unducted airflow conditions.

» **RoHS Compliant**

For further technical information, please contact Advanced Thermal Solutions, Inc. at **1-781-769-2800** or **www.qats.com**

$$T_j = 0.9 \times (124 - 20) + 20 = 113.3\ ºC \qquad (6)$$

Therefore, the junction temperatures to be determined by different analyses must be less than 113.3ºC at an ambient of 20ºC.

Analytical Analysis

As a starting point, an LED junction temperature of 108ºC is assumed, with a required forward current of 1000 mA. The usable light tool [3] gives a light efficiency of 9.4% and electrical power dissipation, P_e, of 3.53 W. The light efficiency is the ratio of the light power, P_l that the LED emits to the electrical power input, P_e. This is also given by Equation 7, which can be re-arranged in the form shown in Equation 8.

$$\eta_l = P_l / P_e \qquad (7)$$

$$P_l = \eta_l P_e \qquad (8)$$

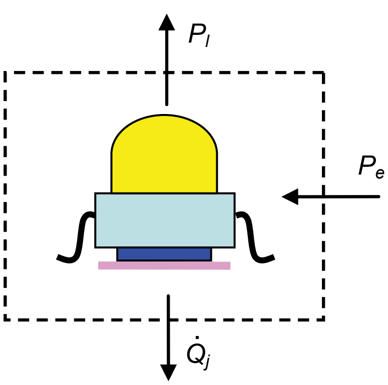

Figure 3. Control Volume Around an LED.

Consider the control volume around the LED in Figure 3. The electrical power input, P_e enters the control volume while the heat dissipated, $\dot{Q}_j$ and the light power, P_l leave the

control volume. Applying an energy balance to the control volume yields Equation 10.

$$\sum E_{in} = \sum E_{out} \qquad (9)$$

$$P_e = P_l + \dot{Q}_j \qquad (10)$$

Re-arranging Equation 10 yields Equation 11:

$$\dot{Q}_j = P_e + P_l \qquad (11)$$

Substituting Equation 8 into 11 yields Equation 12. Re-arranging Equation 12 gives Equation 13:

$$\dot{Q}_j = P_e - \eta_l P_e$$

$$\dot{Q}_j = P_e (1 - \eta_l)$$

(13)

Because all other values of Equation 13 are known, the heat dissipated by the LED can be calculated.

(12)

$$\dot{Q}_j = 3.53 \times (1 - 0.094) = 3.2\ W \qquad (14)$$

Standard FR-4 boards can be used for LEDs with up to 0.5 W of dissipation, but metallic substrates are required for higher levels [4]. Because the LED heat dissipation is 3.2 W, a metal core board type PCB was used. Figure 4 is a sketch of the LED junction to heat sink. It shows each material that the heat from the LED must transfer through before it reaches the heat sink. Figure 4 also provides a thermal resistance diagram based on the sketch. The resistances are considered to be in series.

The metal core board's spreading resistance, $R_{metalcore}$ can be determined using the spreading resistance calculation method explained in [5]. The effective in-plane thermal conductivity can be calculated using Equation 15, as described in [6]:

where t is the total thickness of the PCB, $t_{c,i}$ and $t_{g,i}$ are the

$$k_{p,e} = \frac{\sum_{i=1}^{N_c} k_c t_{c,i} + \sum_{i=1}^{N_g} k_g t_{g,i}}{t} \qquad (15)$$

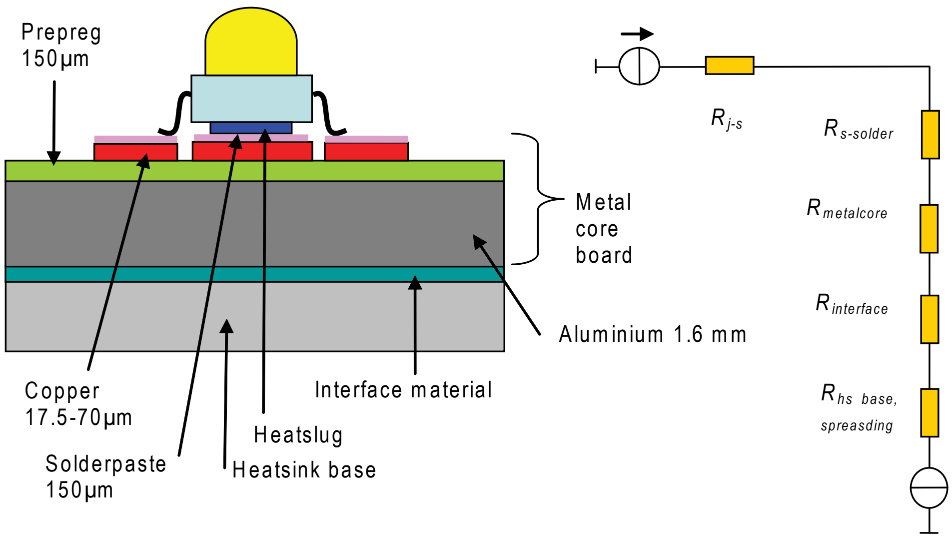

Figure 4. Heat Sink-to-LED Junction and Corresponding Thermal Resistance Diagram.

thicknesses of the copper and glass-epoxy or prepreg/dielectric layers, and k_c and k_g are the thermal conductivities of the copper and glass-epoxy, respectively.

Equation 15 can be modified to accommodate the PCB's aluminum layer, as shown in Equation 16. Additionally, the coverage percentage of each layer can be taken into account by the factor β_i,

$$k_{p,e} = \frac{\sum_{i=1}^{N_c} \beta_i k_c t_{c,i} + \sum_{i=1}^{N_g} \beta_i k_g t_{g,i} + \beta_{AL} k_{AL} t_{AL}}{t} \qquad (16)$$

where t_{AL} is the aluminum thickness and k_{AL} is the thermal conductivity of the aluminum.

The PCB's material properties are shown in Table 3. Using the spreading resistance calculation and effective in-plane thermal conductivity methods previously mentioned, along with the PCB's material properties, the spreading resistance in the metal core board was calculated as $R_{metalcore}$ = 1 K/W.

Material	Coverage [%]	Conductivity [W/m·K]	Thickness [µm]
Copper	50	385	70
Dielectric	100	3	150
Aluminum	100	180	1600

Table 3. PCB Material Properties.

The other thermal resistance needs are as follows:

1. $R_{s\text{-}solder}$ is the thermal resistance in the solder under

the LED slug. It is 146 µm thick with a thermal conductivity of 50 W/m·K and an area of 22.5 mm². This results in a thermal resistance of 0.13 K/W.

2. The interface resistance is assumed to be 0.2 K/W. This is comparable to the resistance of Chomerics T405-R thermal interface material.
3. The spreading in the heat sink base, $R_{hs\ base,spreading}$ is assumed to be zero.
4. The junction-to-heat slug thermal resistance of the LED is 9 K/W [1].

Consider the thermal resistance in the heat transfer path from the junction to the heat sink base shown in Figure 4. These resistances are considered to be in series, and the junction-to-heat sink resistance is the sum of the individual resistances. Using Fourier's law of heat conduction in a one-dimensional differential form, the heat transfer rate between the junction and the heat sink can be expressed by Equation 17. Because the required lifetime junction temperature, the heat dissipated by the LED, and the thermal resistance from the junction to heat sink are known, Equation 17 can be re-arranged to calculate the heat sink temperature, Equation 18.

$$\dot{Q}_j = \frac{T_j - T_{hs}}{R_{j-hs}} \qquad (17)$$

$$T_{hs} = T_j - \dot{Q}_j R_{j-hs} \qquad (18)$$

$$T_{hs} = 113.3 - 3.2 \times 10.3 = 80.34\ ^{o}C \qquad (19)$$

Because there are three LEDs on the heat sink, the sink must be able to transfer 3 x 3.2 W = 9.6 W from a heat sink temperature of 80.34ºC to an ambient of 20ºC. Using the thermal resistance diagram shown in Figure 5, the thermal resistance from the heat sink to ambient can be calculated using Equation 21. From Equation 22, the heat sink thermal resistance must be less then 6.28 K/W or the heat sink must be able to dissipated 9.6 W at a temperature difference of 60.34 K.

$$\dot{Q}_{hs} = \frac{T_{hs} - T_{amb}}{R_{hs-amb}} \qquad (20)$$

$$R_{hs-amb} = \frac{T_{hs} - T_{amb}}{\dot{Q}_{hs}} \qquad (21)$$

$$R_{hs-amb} = \frac{80.34 - 20}{9.6} = 6.28\ K/W \qquad (22)$$

Figure 5. Thermal Resistance Diagram of LED Junction to

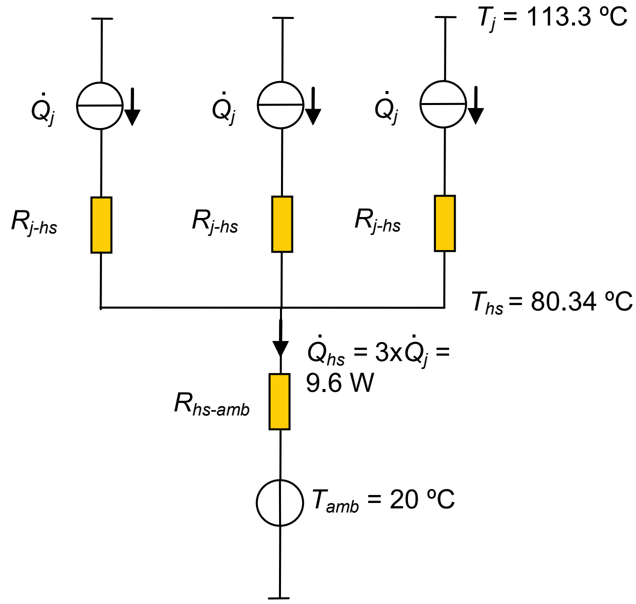

Ambient.

For the analytical simulation, two methods available to determine the heat sink thermal resistance. The first is to refer to the heat sink's data sheet, which, in this study, shows that 9.6 W can be dissipated at a 56.3K temperature difference (see Figure 6.) This is less than the required 63.4 K temperature difference.

The second method is to use an analytical model of the heat sink (whose part number is ATSEU-077B-C4-R0.) The results of the analytical analyses are shown in Table 4.

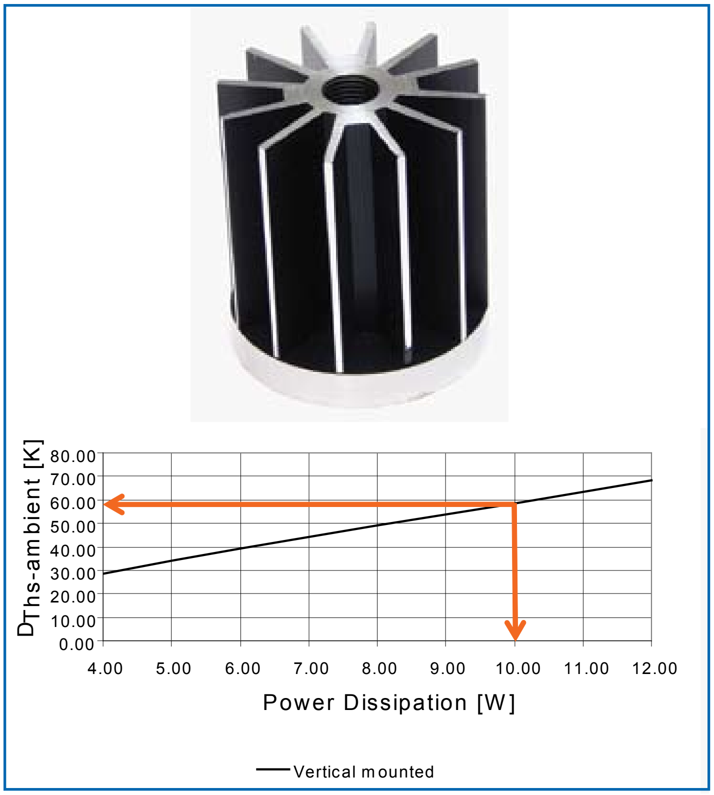

Figure 6. Experimental Results using the ATSEU-077B-C4-R0 Heat Sink.

Numerical Results

Based on the analytical results, a model of the downlight was created. It was simulated in a free air environment. The boundary conditions for a free air environment are discussed in [7]. The results of the numerical analysis are shown in Table 4.

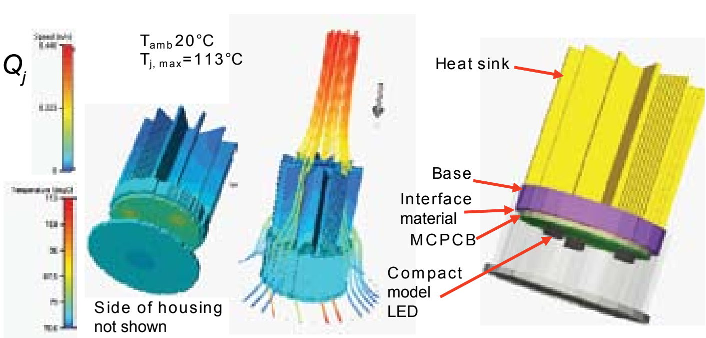

Figure 7. Numerical Results of the Downlight Analysis.

Experimental Results

An experimental model of the downlight was manufactured and tested. This was done in order to verify the results of the analytical and numerical analyses. The LEDs were calibrated using the forward voltage method, also referred to as the electrical method. In the forward voltage method, the LED is calibrated at a sense current. Thereafter, the LED is tested at the required forward current of 1000 mA. When steady-state has been reached, the junction voltage at the sense current is measured and the junction temperature can be calculated from the calibration curve. A detailed example of the forward voltage/electrical test method is given in [8].

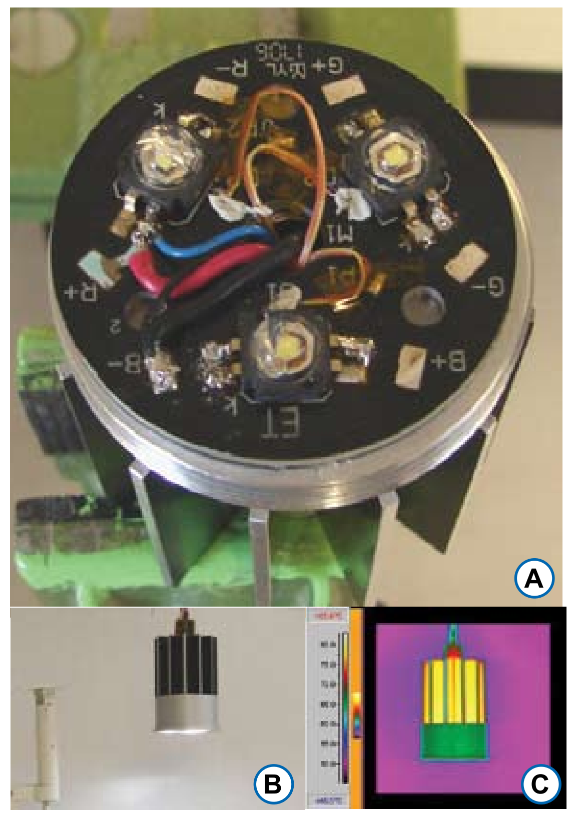

Figure 8. Images of the Experimental Analysis showing the LEDs (a), the Experimental Set Up (b) and an Infrared Picture of the Lighting System (c).

Comparing the Analytical, Numerical and Experimental Results

Table 4 summarizes the analytical, numerical and experimental results for the LED lighting system. The table shows that the results obtained using the different methods are within 10% of each other and have a high confidence level. The maximum temperature difference calculated for the CFD results is 93 K. Further, the experimental results

Table 4. Comparison of the Analytical, Numerical and Experimental Data, Normalized to an Ambient Temperature of 20ºC.

Parameter	Units	Analytical, with experimental hs-data	Analytical, only	CFD	Experimental
$T_{ambient}$	°C	20	20	20	20
$I_{forward}$	mA	1000	1000	1000	1000
Light efficiency	%	9%	9%	9%	9%
$P_{dissipated,total}$	W	9.6	9.6	9.6	9.6
$T_{heatsink\ base}$	°C	68	76	75	71
T_{board}	°C	73	81	84	78
$T_{j,\ led}$	°C	102	110	113	107
Comparison of methods	%	95%	103%	105%	100%
$\Delta T_{j\text{-}amb}$	K	82	90	93	87
Less than the required temperature difference of 93.6K		TRUE	TRUE	TRUE	TRUE

have a temperature of 87 K. Both of these results are below the required 93.6 K for the lifetime condition. Therefore, the analyses have shown that the LED-based downlight system satisfies the lifetime temperature condition. The LED-based downlight lighting system end product is shown in Figure 9.

Figure 9. LED-based Downlight Whose Cooling Solution was Developed by ATS Europe B.V.

Summary

This article explains the development of an LED-based downlight system. The LED lighting system uses 3 LUXEON K2 LEDs at a forward current of 1000 mA. The article discusses analytical, numerical and experimental analysis methods A comparison of the different analysis results are given. For reliability, it is recommended that at least two independent results be obtained, and that these not differ by more than 20%.

References:

1. Luxeon K2 Technical data sheet, DS51, http://www.philipslumileds.com/pdfs/DS51.pdf, September 2009.
2. Luxeon K2 Reliability Datasheet RD06, http://www.philipslumileds.com/pdfs/RD06.pdf, September 2009.
3. Future Electronics, Usable Light Tool, www.futurelightingsolutions.com.
4. Petroski, J., Thermal Challenges in LED Cooling, Electronics Cooling Magazine, November 2006.
5. Spreading Thermal Resistance: Its Definition and Control, Qpedia eMagazine, September 2007.
6. Shabany, Y, Component Size and Effective Thermal Conductivity of Printed Circuit Boards, ITHERM, 2002.
7. Boundary Conditions for Natural Convection CFD Simulations, Qpedia eMagazine, June 2009.
8. Hulett, J. and Kelly, C., Measuring LED Junction Temperature, http://www.photonics.com/Content/ReadArticle.aspx?ArticleID=34316, September 2009/

First Volume of Qpedia Thermal eMagazine Articles Now Available in Hardcover Book

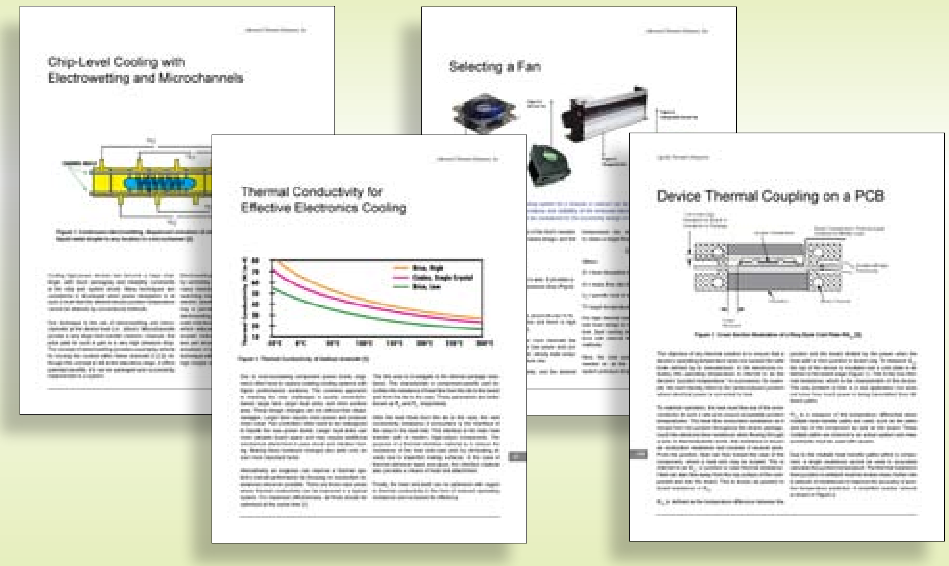

$94.95
On Sale Now!

Visit www.qats.com, email qpedia@qats.com or call 781-769-2800 to place your order!

Advanced Thermal Solutions, Inc. (ATS) has published Qpedia Thermal eMagazine, Volume 1, Issues 1-12, a hardbound, full-color book that compiles all of the electronics thermal management articles that first appeared in its online emagazine, Qpedia. In all, the book contains 46 technically comprehensive articles offering expert-level coverage on a wide range of heat management issues that impact virtually all of today's electronic devices. Topics range from spot cooling hot areas on silicon dies to enhancing airflow over PCBs and inside chassis and cabinets.

All articles are written and edited at the engineer-level by the thermal and mechanical engineers from Advanced Thermal Solutions, including Kaveh Azar, Ph.D., the company's president and CEO; and Bahman Tavassoli, Ph.D., its chief technologist. Both Azar and Tavassoli are internationally recognized experts in the thermal management of electronics.

Qpedia Thermal eMagazine, Volume 1, Issues 1-12, ISBN-978-0-615-23660-5, the hardbound, full color book can be ordered for $94.95 (USD) by calling 781-769-2800 or by email qpedia@qats.com.

Volume discounts for organizations and academic institutions are also available. Contact ATS or visit www.qats.com for details.

Advanced Thermal Solutions, Inc.
89-27 Access Road | Norwood, MA | USA
T: 781.769.2800 | F: 769.769.2800 | www.qats.com

Thermal Transient

Response of Low Power Cabinets

Rooms that contain telephone switching equipment usually have an environmental control system to ensure that all equipment work at their preferred temperature and humidity. This control system typically can cool a telecommunication room that has equipment heat load in the enclosure and thermal load from accessory devices, under the worst conditions. The air conditioning system could fail due to a utility power outage, fan failure or a chiller system malfunction. The failure of a cooling system will increase the temperature of both the equipment and the temperature, which will lead to system failure and service interruption.

Telecommunication cabinets in the field use fans and vents to maintain a proper working environment. Along with absorbing the thermal load from devices, the cabinets take in solar radiation from the surrounding environment. In some cabinets, solar radiation has a huge effect on the internal temperature because thermal loading from the radiation may exceed the heat flux generated by devices themselves. Variation of environmental temperature also has a large impact because it determines the intake air temperature. A cooling system outside a cabinet can also fail due to fan outage or vent choking.

The electrical equipment inside a telecommunications cabinet in a building or in the field is designed to work in ambient air no higher than 50˚C (122˚F). The transient thermal response of a cabinet determines how long its systems can operate without a cooling system. Repairing a cooling system can take several hours or days depending on the severity of the outage. But, most cooling system outages can be fixed within hours if the problem is quickly identified. A telecommunications cabinet should be designed to maintain its functions as long as possible, if there is a short time cooling system outage.

An experimental investigation was conducted on the transient air temperature inside a No 5 ESS center cabinet under different heat loads. It was found that the transient thermal response is a function of power dissipation. The effects of cabinet mass, solar radiation and environmental temperature on the air temperature inside the cabinet were also numerically studied.

The test facility is shown in Figure 1. It consists of a thoroughly-instrumented, full scale model of a segment of the container. The facility is capable of simulating the thermal response of cabinets with heat loading from 35 to 700 W/m^3 (1 to 20 W/ft^3).

Figure 1. Interior of Test Container

Figure 2 shows the measured air temperature with respect to time at different internal power dissipation levels. The rate of temperature rise is a function of time duration and power dissipation. A regression analysis of the experimental data gives the expression:

$$T = T_0 + 0.00229Qt^{(0.79+0.000142Q)} \qquad (1)$$

Where, T_0 is the equilibrium temperature inside the cabinet prior to the shutdown of the cooling system, Q is the total power dissipation of the system in W/m^3, and t is the time in minutes.

The temperature rising rate is a function of time and heat dissipation:

$$\frac{dT}{dt} = 0.00229Q(0.79 + 0.000142Q)\frac{1}{t^{0.21-0.000142Q}} \qquad (2)$$

Where the $\frac{dT}{dt}$ is inversely proportional to $t^{0.21-0.000142Q}$.

At the beginning of the cooling system outage, the increasing air temperature rate is at its largest; then the value of $\frac{dT}{dt}$ gradually decreases over time. The trend of temperature is clearly illustrated in Figure 2. The rate change of temperature increase can be explained by the heat transfer between the cabinet wall and the outside environment. At the onset of a cooling system outage, the devices and air inside the cabinet come out of their thermal equilibrium state and the generated heat causes the internal temperature to rise quickly. As the inside frame, air and wall temperatures increase with time, more heat is transferred from the wall exterior to the outside by convection and radiation. Because the thermal capacity of the cabinet is a constant, the rate of increase of the interior temperature will slow with time as more heat is lost to the outside environment. This heat loss is due to the increasing temperature difference between the cabinet and the outside environment.

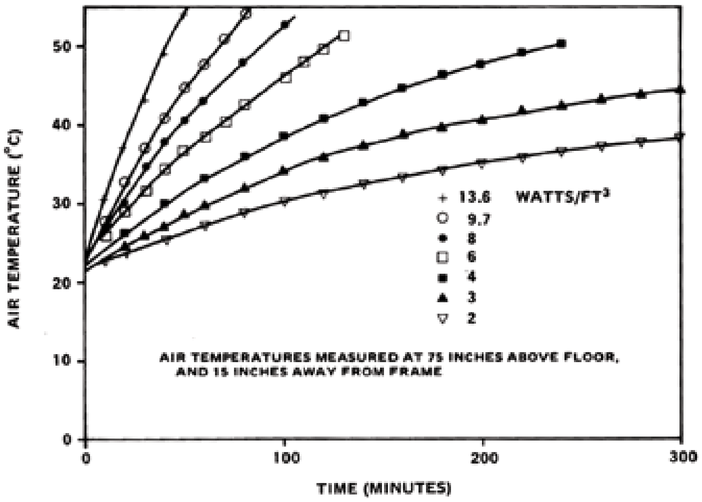

Figure 2. Transient Temperature Curve for Different Power Dissipation

The time it takes for the air temperature to reach 50˚C, as extracted from Figure 2, is compared with a numerical calculation in Figure 3. For heat dissipation equal to or less than 105 W/m^3 (3 W/ft^3), the elapsed time to reach 50˚C is more than 6 hours. On the other hand, it takes only 43 minutes for air to reach 50˚C under 476 W/m^3 (13.6 W/ft^3) of heat dissipation.

In the absence of an operating cooling system, the sealed cabinet works as volume with the internal heat source. If this volume is treated as a lump sum of mass, the total mass of the cabinet also has an impact on its transient temperature response. Figure 4 shows the elapsed time required for a cabinet with different a power/mass ratio to reach 50˚C. Obviously, at the same power dissipation the

cabinet with larger mass requires a longer time to reach critical temperature.

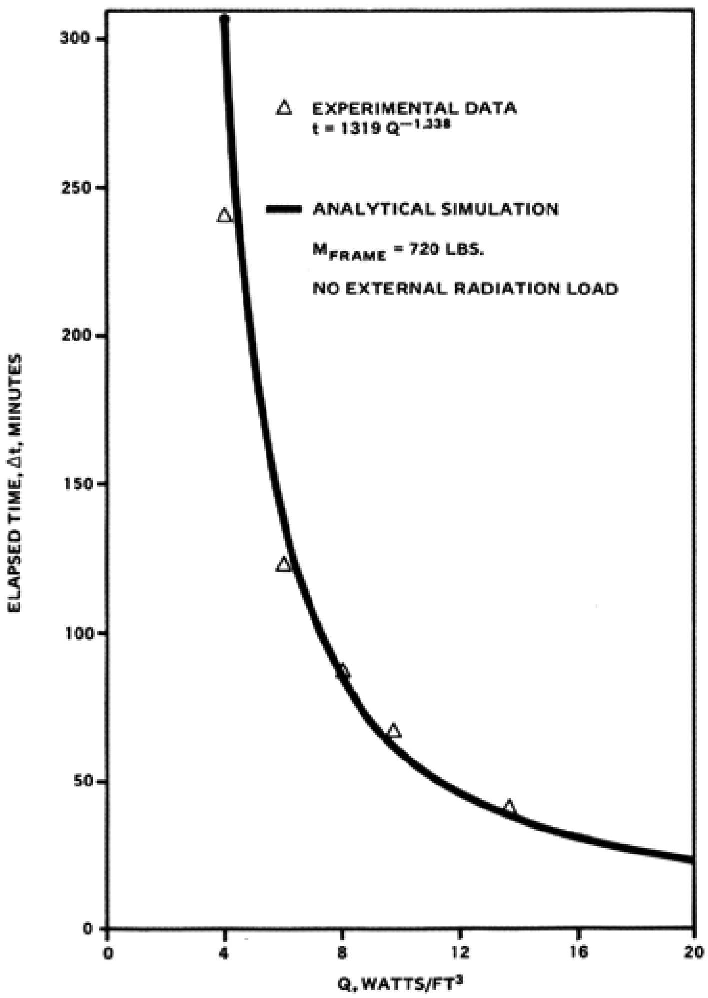

Figure 3. Dependence of Elapsed Time to 50˚C Air Temperature on Power Dissipation

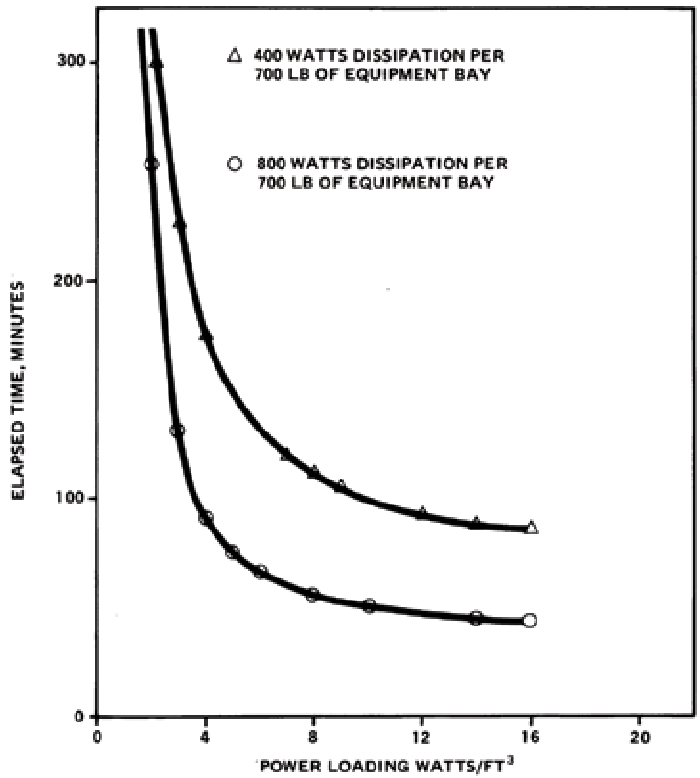

Figure 4. Variation of Elapsed Time with Power Dissipation and Frame Mass

Figure 5 shows the effect of solar radiation load on a cabinet with 70 W/m³ (2 W/ft³) loading. The dotted line curve represents temperature without solar radiation. The solar loading is a function of time with sunrise at 0 minutes and noon at 300 minutes. The absorptivity of the cabinet varies from 0.1 to 0.4. The solar radiation doesn't make much difference at the inception of the process, but it causes a large temperature rise in the afternoon. In cases of absorptivity larger than 0.2, the solar radiation has its largest effect at 500 minutes.

Figure 6 shows that a 10˚C temperature variation is attained in the enclosure during daylight hours, regardless of power dissipation. The observation can be applied to a cabinet working in the field.

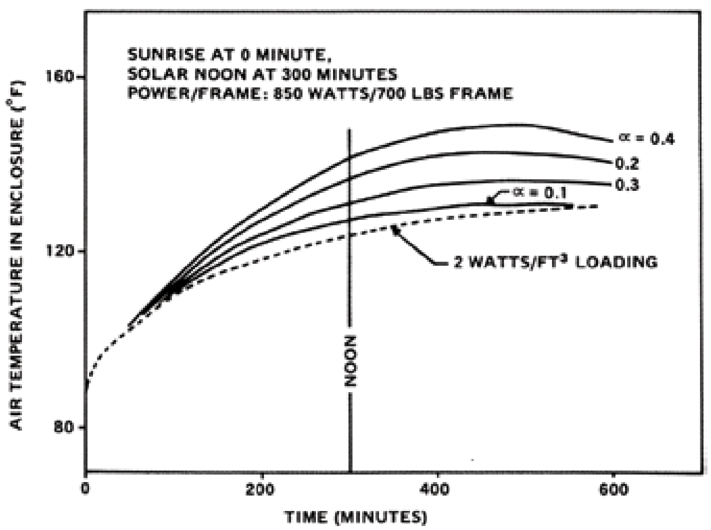

Figure 5. Influence of Solar Radiation on Response of Enclosure

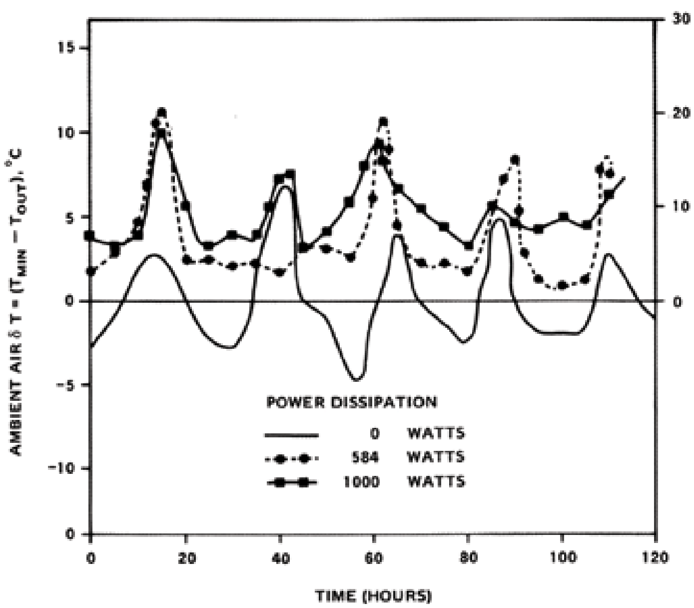

Figure 6. Hourly Variation of Indoor and Outdoor Temperature Difference

The transient temperature response of a closed cabinet without a cooling system is mainly determined by the power dissipation rate and system mass. The time needed to reach the 50˚C threshold for a tested cabinet decreases asymptotically with an increase of the power dissipation level. For power dissipation larger than 280 W/m^3 (8 W/ft^3), the elapsed time is less than 90 minutes. At such a power level, a temporary cooling system outage will cause the equipment to overheat in a short period. For prevention purposes, passive cooling methods are recommended when designing such systems. Solar radiation and environmental temperature also have major effects on a cabinet's internal temperature, especially for cabinets working in the field. In some geographical locations, such as Arizona or New Mexico, the radiation heat flux can be as high as 1200 W/m^2 (110 W/ft^2) and daytime temperature variation can reach 20˚C. Extra consideration should be given for the design of cabinets working in this kind of environments. Solar shielding and extra venting have proven to be effective solutions for reducing the influence of solar radiation on electronic devices inside cabinets.

ATS ADVANCED THERMAL SOLUTIONS, INC.
Innovations in Thermal Management®

superGRIP™

HEAT SINK ATTACHMENT FOR DENSELY POPULATED PCBS

- Provides tight, secure heat sink attachment in shock and vibration environments
- Occupies minimal area around chip, allowing its use in densely populated PCBs
- Allows the heat sink to be detached and reattached without damaging the component or the PCB
- Strong, uniform attachment force helps achieve maximum performance from phase-changing TIMs

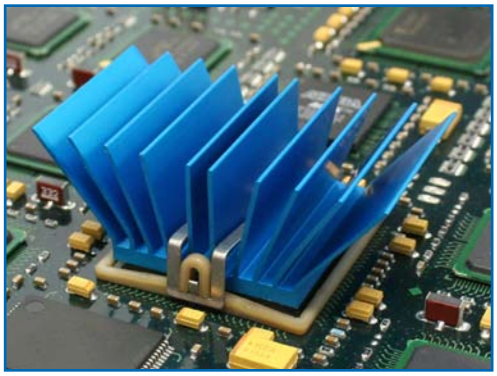

ATS' superGRIP™ frame and spring clips are Patent Pending.

About superGRIP™

ATS' superGRIP™ is a new two-component, attachment system which quickly and securely mounts heat sinks to a wide range of hot running Ball Grid Array (BGA) components, while using a minimal amount of space on the PCB and eliminating the need to drill holes.

The two-part superGRIP system features a plastic frame clip that fastens securely around the perimeter of a component and a metal spring clip which slips through the heat sink's fin field and locks securely to both ends to the plastic frame. The resulting superGRIP assembly applies steady, even pressure to the component throughout the product lifecycle, improving thermal performance and long-term reliability.

With this latest edition, ATS now offers two tiers of heat sink clip attachment: maxiGRIP™, for general purpose and high performance applications: and superGRIP, for high performance applications with densely populated PCBs and little space around the component for mechanical attachment.

ATS' superGRIP heat sink attachment system permits the use of high performance phase changing thermal interface materials that improve heat transfer by as much as 20 times more than typical double-sided adhesive thermal tapes. It also allows for the heat sink to be detached and reattached without damaging the component or the PCB, an important feature for applications where PCB rework and ease of assembly and disassembly are important.

The superGRIP system is available with ATS' maxiFLOW™ family of heat sinks which feature a low profile, spread fin architecture to maximize surface area for more effective convection (air) cooling. Testing at an air flow rate of just 0.5 m/s (100 ft/m) shows that device junction temperatures (Tj) can be reduced by more than 20 percent below the temperatures achieved using heat sinks with traditional fin styles.

It is also available with ATS' straight fin and cross cut heat sinks, as well as additional sizes and configurations, as custom options.

For more information about ATS' high performance heat sink products with superGRIP clip attachment, lead times and pricing, please visit www.qats.com or call 781-769-2800.

superGRIP FEATURES:

» **Minimal Keep Out Area**
Requires minimal space around the component's perimeter; ideal for densely populated PCBs

» **Improves Performance**
superGRIP's strong, uniform attachment force helps achieve maximum performance from phase changing thermal interface materials

» **Easy Installation and Removal**
Allows heat sink to detached and reattached without damaging the PCB.

» **Thermal Interface Material**
Comes standard with clean-break, reworkable, Chomerics T-766 phase change material

» **Frame Clip**
Made from plastic resins that allow it to be thin, yet incredibly strong

» **Spring Clip**
Flat, twin-channel clip, made from 300 series stainless steel, provides strong retention forces

» **No Special Tools Needed**
Frame and spring clips can both be installed by hand or with common hand tools such as a flat blade screwdriver

» **maxiFLOW™ Heat Sink**
Available with maxiFLOW heat sinks which maximize surface area for more effective convection (air) cooling

» **Custom Options**
Clips and heat sink can be customized in different sizes

Single-and Two-Phase Flow

Calculations for Small Channels

Increasingly powerful electronic devices are pushing traditional air cooling technology to its performance limit. It is increasingly difficult to design cost-effective air-cooled heat sinks that can dissipate more than 100 W/cm^2 heat flux at the device level [1]. The increasing volume of air cooled heat sinks also prevents their application as miniaturization becomes the trend in the electronic industry. Liquid cooled heat sinks have emerged as the natural substitute for air cooled heat sinks because of their better performance and smaller size. The most commonly used working fluid is water. Extensive studies show that for use in liquid cooling systems, water provides more stable properties and higher thermal capacity than other fluids.

Thermal Benefits of Liquid Cooling in Small Channels

The ability of liquid cooled heat sinks to dissipate heat is determined by heat conduction in solids and heat convection in fluids. Normally, convection is the dominant factor for reducing thermal resistance when a highly conductive material is used to fabricate heat sinks. In most cases, the single-phase flow of liquid inside minichannels and microchannels is a laminar flow. For a fully developed laminar flow in a square channel with constant wall temperature or constant wall heat flux, the Nusselt number is a constant. The heat transfer coefficient can be calculated by the following equation,

$$h = \frac{Nuk}{D_h} \Rightarrow h \propto \frac{1}{D_h} \qquad (1)$$

The heat transfer coefficient is inversely proportional to the channel hydraulic diameter, D_h. By reducing the channel hydraulic diameter, a large heat transfer coefficient can be achieved. On the other hand, the friction factor for a fully developed laminar flow in a square channel is also a constant. The pressure drop across the channel is determined by the equation,

$$\Delta P = 4f\left(\frac{\rho u^2}{2}\right)\frac{L}{D_h} \qquad (2)$$

The pressure drop is also inversely proportional to the channel hydraulic diameter at constant average flow velocity. The pumping power, W_p needed to drive the flow through the channel is defined by the equation,

$$W_p = Q \cdot \Delta P \qquad (3)$$

Where Q is the volumetric flow rate.
For a constant volumetric flow rate, the pumping power can be calculated by the following equation:

$$W_p = Q \cdot 4f\left(\frac{\rho u^2}{2}\right)\frac{L}{D_h} = 2f\rho Q^3 L \frac{1}{D_h^5} \Rightarrow W_p \propto \frac{1}{D_h^5} \qquad (4)$$

The pumping power needed increases dramatically if the channel hydraulic diameter decreases. There are two solutions for reducing the required pumping power. One is to use a high aspect ratio rectangular channel, which increases the wetted and channel cross-section area and keeps the channel hydraulic diameter reasonably small at the same time. The second solution is to stack many channels together to form multiple layers. Compared with single layer heat sinks, multilayer heat sinks keep the individual channel hydraulic diameter unchanged, but increase the total wetted and cross-sectional area multiple times.

Due to its broad application in boilers, power plants, and refrigerant systems, boiling in conventional size tubes has been extensively investigated by many researchers. In the past twenty years, the boiling process and two-phase flow in small channels have attracted growing interest due to the need for high heat flux dissipation and the miniaturization of electronic devices. Because of our insufficient knowledge of flow patterns and boiling correlations, two-phase flow in small channels is difficult to predict and therefore difficult to implement in electronic devices.

The key issue of two-phase flow research is predicting the local boiling heat transfer coefficient. Two important heat transfer mechanisms are normally considered for modeling the boiling in channels: nucleate boiling heat transfer and convective boiling heat transfer. Nucleate boiling in channels is similar to nucleate pool boiling except for the effect of bulk flow and the influence of channel size and geometry. Bulk flow affects the growth and departure of the bubbles and bubble-induced convection. The channel size affects the flow pattern, which influences the dominant heat transfer mechanism. Convective boiling refers to the interaction between the channel wall and the liquid-gas mixture. In conventional size channels, the nucleate boiling strongly depends on local heat flux. It tends to be dominant at low vapor quality and high heat flux conditions. Convective boiling is mainly dependent on local vapor quality and mass flux. It is dominant on high vapor quality and low heat flux conditions.

For channels of conventional size, Chen [2] suggested the local two-phase boiling heat transfer coefficient, h_{tp} to be a superposition of the nucleate boiling coefficient, h_{nb} and the convective boiling coefficient, h_{cb} with proper factors.

$$h_{tp} = Sh_{nb} + h_{cb} = Sh_{nb} + Eh_l \tag{5}$$

The nucleate pool boiling coefficient, h_{nb} is given by Forster and Zuber [3], the single-phase convective heat transfer coefficient, h_l is given by Dittus and Boelter [4], and the function of E and S were provided by Chen [2].

For boiling minichannels and microchannels, surface tension, which is normally negligible in large size channels, begins to play an important role in two-phase flow. This makes the boiling in small channels more complicated than that in conventional size channels. Lazarek and Black [5], Tran et al. [6], Kandlikar [7], Warrier et al. [8], and Yu et al. [9] have proposed different boiling heat transfer coefficient correlations based on their experiments. The research of Lei et al. [10] shows that Yu's correlation is best fit with boiling test results in square channels of 0.5 mm hydraulic diameter.

Heat Transfer Coefficient in Single-Phase Flow

In minichannels and microchannels, the flow regime is laminar as long as $Re_D < 1400$, which is true for most cases. The local heat transfer coefficient is related to the flow condition, channel geometries, and hydraulic and thermal entrance length. When water is used as the working fluid, the thermal entrance is the dominant length scale.

The hydraulic entrance length, L^+_{hy} for laminar flow, and the thermal entrance length, L^*_{th} for uniform wall heat flux with a fully developed laminar velocity profile recommended by Shah and London [11] for a rectangular channel are, listed in Table1.

Table 1. L^+_{hy} and L^*_{th} for Rectangular Channels.

Aspect ratio α	L^+_{hy}	L^*_{th}
1	0.090	0.066
2	0.085	0.057
4	0.075	0.042

The aspect ratio, α is defined as:

$$\alpha = \frac{b}{a} \tag{6}$$

CLWT-067

BENCHTOP, CLOSED LOOP WIND TUNNEL FOR ELEVATED TEPERATURE TESTING OF BOARDS AND COMPONENTS

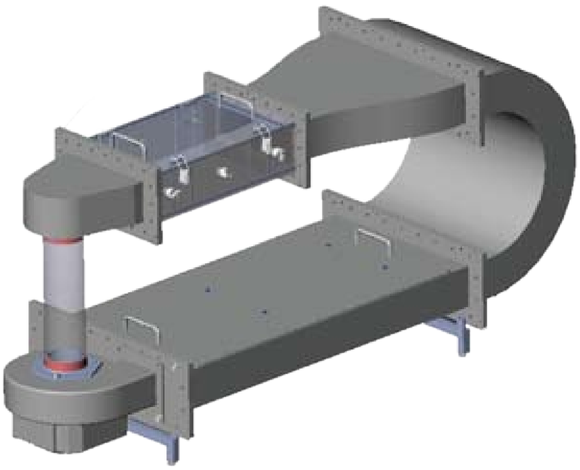

The CLWT-067 is a research-quality closed loop wind tunnel that provides a convenient, accurate system for thermally characterizing PCBs and individual components at controlled temperatures from ambient to 85°C.

The CLWT-067 wind tunnel produces air flows up to 7 m/s (1378 ft/min). With customization, it can generate flows up to 50 m/s (10,000 ft/min) using orifice plates (available optionally). The clear Lexan test section lets the user to view the test specimen and allows for flow visualization.

Unlike open loop wind tunnels, the CLWT-067 re-circulates internal air. This allows the system heater to quickly warm the air to a specific temperature. The testing of boards and components in hot air is a requirement in some NEBS and other standards. The precise controls and temperature range of the CLWT-067 wind tunnel allows its use for testing heat sink performance and for calibrating air and temperature sensors.

The complete wind tunnel fits on most lab benches and is powered from standard AC outlets. It has a smaller footprint than traditional, closed loop wind tunnels or environmental test chambers.

The wind tunnel's test section can be accessed from the top door for mounting and repositioning of boards, components and sensors. Internal rail guides provide an easy mechanism to install test specimens of different sizes (e.g., PCB, heat sink).

Instrument ports (6) are provided in the side walls of the test section for placing temperature and velocity sensors such as thermocouples, Pitot tubes and hot-wire anemometers.

Custom options are also available. Contact ATS for details.

OVERALL DIMENSIONS (L X W X H)
143.6 cm x 49.3 cm x 67.7 cm
(56.5" x 19.4" x 26.6")

TEST SECTION DIMENSIONS
41.8 cm x 22.5 cm x 9.5 cm
(16.4" x 8.9" x 3.7")

MATERIALS
SHEET METAL, LEXAN

FLOW RANGE
0 TO 7 m/s (1378 ft/min)

TEMPERATURE RANGE
Up to 85°C (185°F)

WEIGHT
70.7 kg (156 lbs.)

For further technical information, please contact Advanced Thermal Solutions, Inc. at **1-781-769-2800** or **www.qats.com**

FEATURES:

- **Quick Access**
  Quickly change the test specimen through the top access test section
- **Sensor Ports**
  Measure pressure, velocity and temperature through the sensor ports
- **Data Center**
  View data and monitor events (with optional controller)
- **Flow Characteristics**
  High quality flow with very low turbulence intensity

APPLICATIONS:

- **High Temperature Testing**
  Evaluate the effects of elevated temperatures on component and PCB response and reliability
- **Heat Sink Characterization**
  Characterize a variety of heat sink sizes for natural and forced convection cooling
- **Sensor Calibration**
  Precision temperature and velocity controls allow accururate calibration of sensors
- **Component Testing**
  Utilize for individual or multiple component testing
- **Multiple PCB Testing**
  Test actual or simulated PCBs for thermal and flow distribution

Where b is channel height and a is channel width.

For example, for water at 23°C, with Pr = 6.46 and Re_D = 500, the dimensional hydraulic entrance length for a square channel is:

$$L_{hy} = L_{hy}^{+} Re_D D_h = 45D_h \quad (7)$$

The dimensional thermal entrance length for a square channel is:

$$L_{th} = L_{th}^{*} Re_D Pr D_h \approx 219D_h \quad (8)$$

The thermal entrance length is much larger than the channel hydraulic diameter. Therefore the entrance length effect cannot be neglected in calculation.

Chandrupatla and Sastri [12] analyzed the simultaneously developing flow inside a square duct with constant wall heat flux. Their results are presented in Table 2.

Table 2 Nu_x as a Function of x for Simultaneously Developing Flow in a Square Duct.*

x*	Nu_x				
	Pr = 0.0	0.1	1.0	10.0	∞
0.0050	14.653	11.659	8.373	7.329	7.269
0.0075	12.545	9.597	7.122	6.381	6.331
0.0100	11.297	8.391	6.379	5.816	5.769
0.0125	10.459	7.615	5.877	5.480	5.387
0.020	9.031	6.353	5.011	4.759	4.720
0.025	8.500	5.883	4.683	4.502	4.465
0.04	7.675	5.108	4.152	4.080	4.048
0.05	7.415	4.826	3.973	3.939	3.907
0.10	7.051	4.243	3.687	3.686	3.686
∞	7.013	3.612	3.612	3.612	3.612

When water temperature changes from 23°C to 40°C, the Prandtl number of water varies from 6.64 to 3.62. Chandrupatla and Sastri's data for $Pr = 10.0$ can be used for square channels.

For example, for a single channel of 0.5 × 0.5 mm with uniform heat flux on the channel walls, when Q = 20.0 ml/min (Re = 694), the calculated local heat transfer coefficients in the fully developed region is in the vicinity 4,400 W/m².˚C. For a rectangular channel, there is no analytical or numerical Nusselt number data for simultaneously developing flow. Therefore the following correlation is used:

$$Nu_x = Nu_x^{'} \cdot G(\alpha)' \quad (9)$$

Where $Nu_x^{'}$ is the Nusselt number for parallel plates in simultaneously developing flow, and G(α)' is the correction factor for rectangular channels proposed by Shah and London [11] for uniform wall heat flux boundary condition:

$$G(\alpha)' = 1 - 2.0421\alpha^{-1} + 3.0853\alpha^{-2} - 2.4765\alpha^{-3} + 1.0578\alpha^{-4} - 0.1861\alpha^{-5} \quad (10)$$

Hwang and Fan [13] obtained an all-numerical finite difference solution of $Nu_x^{'}$ for the parallel plate in simultaneously developing flow with uniform heat flux boundary conditions. Their results for Pr = 10.0 are shown in Table 3,

Table 3 $Nu_x^{'}$ as a Function of x^* for Parallel Plate Channel for Simultaneously Developing Flow.

x^*	$Nu_x^{'}$ Pr=10.0
0.000050	50.74
0.000125	34.07
0.000438	20.66
0.00075	17.03
0.00200	12.60
0.00625	9.50
0.010	8.80

Hwang and Fan's data can be used for a parallel plate channel for $x^* \leq 0.01$. The correlation recommended by Shah [14] for parallel plates for thermally developing flow is recommended and the Nu_x is,

$$Nu_x = 8.235 + 8.68(1000x^*)^{-0.506}\exp(-164x^*) \quad (11)$$

Heat Transfer Coefficient in Two-Phase Flow

For two-phase heat transfer coefficient in small channels, the correlation of Yu et al. [9] is recommended.

$$h_{tp} = 6.4 \times 10^6 (Bo^2 We_l)^{0.27} \left(\frac{\rho_l}{\rho_g}\right)^{-0.2} \quad (12)$$

The boiling number, Bo is,

$$Bo = \frac{q}{h_{lg} G} \quad (13)$$

Where G is mass flux and h_{lg} is latent heat.
The Weber number, We_l is defined based on liquid:

$$We_l = \frac{G^2 D_h}{\rho_l \sigma} \quad (14)$$

The ρ_l and ρ_g are the density of liquid and vapor respectively.

For a single channel of 0.5 × 0.5 mm, with uniform heat flux on channel walls with Q = 5.0 ml/min and q" = 750 kW/m^2 (G = 333.3 kg/m^2.s and Bo = 0.00099), the calculated local heat transfer coefficient is in the vicinity of 32,000 W/m^2.˚C. Compared with single-phase flow with a flow rate of 20 ml/min ($\bar{h}$ = 4,400 W/m^2.˚C), the boiling heat transfer coefficient is 6 times higher. The drawback of two-phase flow is that the pressure drop is also several times higher than with single-phase flow. Research is being done on the effects of channel geometry and flow patterns on two-phase flow and heat transfer. Based on the high heat transfer coefficient on the boiling regime, researchers are expecting some interesting results.

Nomenclature:

a channel width (m)
b channel height (m)
Bo boiling number
D_h hydraulic diameter of channel (m)
f friction factor
G mass flux (kg/m^{2}s)
h heat transfer coefficient (W/m^2˚C)
h_{nb} nucleate boiling heat transfer coefficient (W/m^2˚C)
H_1 single-phase convective heat transfer coefficient (W/m^2˚C)
h_{cb} convective heat transfer boiling coefficient (W/m^{2}K)
h_{tp} local two-phase boiling heat transfer coefficient (W/m^2˚C)
k liquid thermal conductivity (W/m˚C)
L channel length (m)
L^+_{hy} hydraulic entrance length (m)
L^*_{th} thermal entrance length (m)
Nu Nusselt number
Pr Prandtl number
Q volumetric flow rate (m^3/s)
Re_D Reynolds number
u flow velocity (m/s)
We Weber number
W_p pumping power (Watts)
ΔP pressure drop across heat sink manifold (Pa)
ρ mass density (kg/m^3)
μ water dynamic viscosity at mean temperature (N·s/m^2)
α channel aspect ratio
σ liquid surface tension

References:

1. Ortega, A., Air Cooling of Electronic Components: Review of Research Developments in the Period 1981-2001 and Their Impact on Our Understanding of Cooling Limits, ASME IMECE, 2003.
2. Chen, J., Correlation for Boiling Heat Transfer to Saturated Fluids in Convective Flow, I & EC Process Design and Development, 1966.
3. Forster, H. and Zuber, N., Dynamics of Vapor Bubble Growth and Boiling Heat Transfer, AIChE J. Vol. 1, 1955.
4. Dittus, E. and Boelter, L., Publications on Engineering, University of California at Berkeley, Vol. 2, 1930.
5. Lazarek, G. and Black, S., Evaporative Heat Transfer, Pressure Drop and Critical Heat Flux in a Small Vertical Tube with R-113, Int. J. of Heat and Mass Transfer, 1982..

6. Tran, T., Wambsganss, M. and France, D., Small Circular- and Rectangular-channel Boiling with Two Refrigerants, Int. J. of Multiphase Flow, 1996.
7. Kandlikar, S. and Steinke, M. Predicting Heat Transfer During Flow Boiling In Minichannels and Microchannels, ASHRAE Trans., 2003.
8. Warrier, G., Dhir, V. and Momoda, L., Heat Transfer and Pressure Drop in Narrow Rectangular Channels, Exp. Therm. Fluid Science, 2002.
9. Yu, W., France, D., Wambsganss, M. and Hull, J., Two-phase Pressure Drop, Boiling Heat Transfer, and Critical Heat Flux to Water in a Small-diameter Horizontal Tube, Int. J. of Multiphase Flow, 2002.
10. Lei, N., Ortega, A., Vaidyanathan, R., Experiments and Modeling of Two-Phase Heat Transfer In Single-layer and Multilayer Minichannel Heat Sinks, Proceedings of the InterPACK Conference, 2007.
11. Shah, R., and London, A., Laminar Flow Forced Convection in Ducts, Advances in Heat Transfer Supplement, Academic Press, 1978.
12. Chandrupatla, A. and Sastri, V., Laminar Flow and Heat Transfer to a Non-Newtonian Fluid in an Entrance Region of a Square Duct with Prescribed Constant Axial Wall Heat Flux, Numerical Heat Transfer 1978.
13. Huang, C. and Fan, L., Finite Difference Analysis of Forced-Convection Heat Transfer in the Entrance Region of a Flat Rectangular Duct, Appl. Sci. Res., 1964.
14. Shah, P., Thermal Entry Length Solutions for the Circular Tube and Parallel Plates, Proc. Natl. Heat Mass Transfer Conf., 3rd, Indian, Inst. Technol., Bombay, 1975.

CFD Analysis of a Heat Sink

Filled with Phase Change Material

Phase change materials (PCM) have been used extensively in thermal management systems. With the advent of Air Force More Electric Aircraft (MEA) Initiative , more and more hydraulic, pneumatic components are being replaced by high power electrical or electronic components [1]. It is anticipated that the heat loads in some of these components exceed 100 W/cm^2. Many conventional systems are too complicated or too costly to implement for some of these applications. Phase change materials are a low cost solution to many application such as discrete or array of components having temporal peak powers. Instead of designing an expensive cooling system, phase change materials can be used for absorbing heat during the short mission applications e.g. a missile [1]. Phase change can also be used in systems within harsh environments. Specifically in [2] the authors considered the application of phase change in heat sinks for using infrared cameras in smoke filled buildings. In this application, the temperature of the environment can reach in excess of 80 ^{o}C. Most of the electronic components inside the camera can not reject heat to the ambient. In fact the system should be isolated from the ambient and heat dissipation from components should go directly to phase change rather than the ambient. The goal of the analysis was to optimize the heat sink to extend the useful life of the phase change.

Solving PCM, using CFD packages, has been the area of many researchers. Wirtz et. al.[3] call their approach a hybrid cooler. They used a semi-empirical method assuming symmetry and a resistance network model. In [4], they modeled the PCM as a lumped slope, using a Flotherm™ CFD package.

In [5] they considered a Carbon foam brazed to Aluminum plates and filled with PCM for reinforcement. They presented a methodology to compute the temperature distribution in this system using a COMSOL Multiphysics Femlab™, a commercially available software. They considered a patented technology using high conductivity reinforced foams created by Oak Ridge National Laboratory and licensed and produced by POCO Graphite of Decatur, Texas. The picture of this foam is shown figure 1.

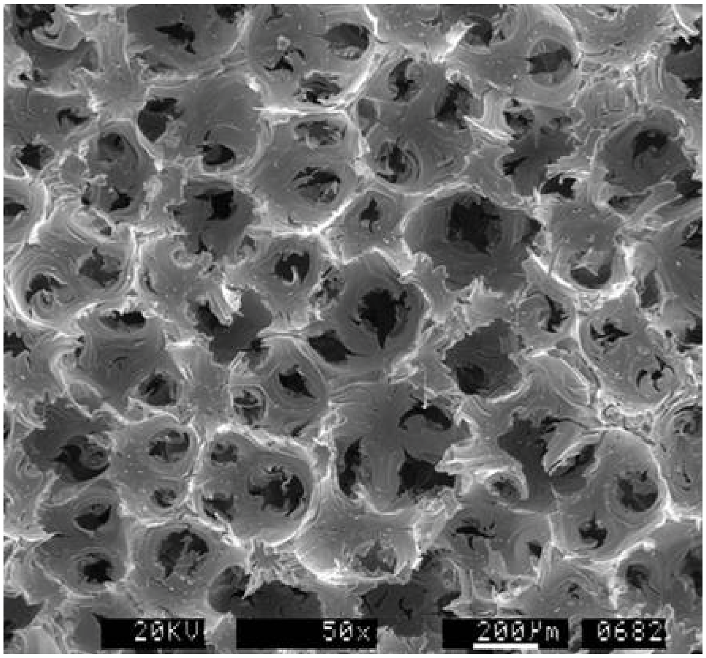

Figure 1. Carbon Foam Microstructure [5].

Commercial high conductivity carbon foams have not been implemented extensively before, because of their low strength, but when mixed with PCM their compressive strength doubles with only a 5% loss in thermal conductivity.

The technique presented by Alawadhi [6] for phase change material is modeled using Femlab. The standard heat equation is written as below:

$$\rho C(T)\frac{\partial T}{\partial t}=\nabla.[k\nabla T(x,t)]+S(x,t)$$

Where,
ρ = Effective density
$C(T)$ = Heat capacity
k = Thermal conductivity
T(x,t) = Temperature as a function of position and time
S(x,t) = Heat source as a function of position and time

The model above can treat the anisotropy of the conduction and also the temperature dependency of the heat capacity of the PCM. Since the electronics are made of silicon carbide, a PCM with a melting point near 200 °C (P-Toulic acid) was selected for this case. Table 1 shows the composition of this simulation.

Table 1. Composition of the Materials Used in the Femlab Simulation [5].

Material	Volume %	Thermal conductivity W/m.K	Density kg/m³	Specific heat capacity J/kg.K
POCO	25%	Out of plane: 135 In plane: 45	550	700
PCM: ptoluic	60%	0.14 near MP	1050	1241
Air at 20 °C	10%	0.0257	1.205	1005
Sic at 20 °C	5%	114	3160	715

The properties are calculated as follows:

Thermal conductivity through the plane and in plane can be calculated as follows:

$$K_Z=\frac{\sum(KZ)_i V_i}{\sum V_i}=39.54\,W/m.K$$

$$K_{XY}=\frac{\sum(Kxy)_i V_i}{\sum V_i}=17.04\,W/m.K$$

The effective density can be calculated as follows:

$$\rho_{eff}=\frac{\sum(\rho)_i V_i}{\sum V_i}=1310\,kg/m^3$$

The heat capacity can be calculated in the same manner:

$$C_p=\frac{\sum(C)_i V_i}{\sum V_i}=1056\,J/kgK$$

Because at the onset of phase change, the heat capacity of the PCM changes, thus the following model can be used:

$$C_{eff}=\begin{cases} C_p & T\le T_m \\ C_P+\frac{L}{\Delta T}\times 0.6 & T_m<T<T_m+\Delta T \\ C_p & T\ge T_m+\Delta T \end{cases}$$

Where,
L = 166.9 KJ/kg
ΔT = 3 °C
T_m = 178.5 °C

The effective capacity is a nonlinear function as shown in figure 2.

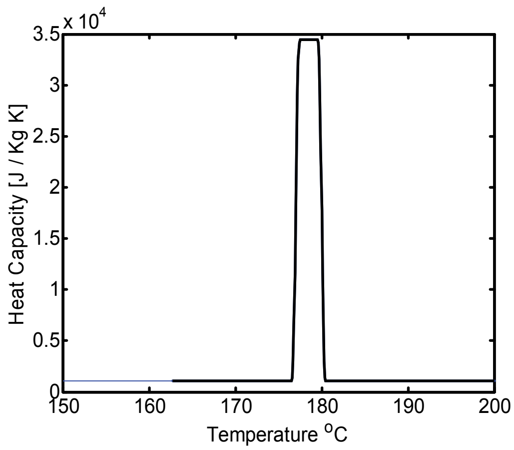

Figure 2. Nonlinear Heat Capacity as a Function of Temperature for Reinforced PCM Filled Carbon Foam [5].

The heat source is composed of two parts. One part is the steady state which is 500 W. The second part is pulses of heat with a duration of 5 seconds and with a peak of 5000 W. They used an element size of 0.8 mm at the top interface and a growth rate of 1.09 to pack more fins close the top. The total number of computational elements were 7454. Figure 3 shows the element distribution derived from the finite element analysis (FEA).

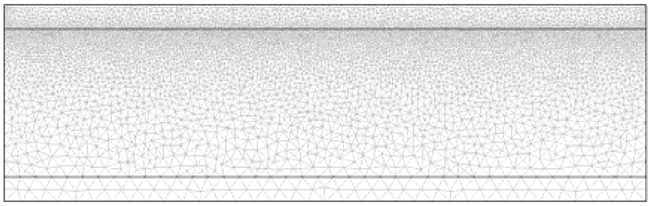

Figure 3. Element Distribution of the Carbon Filled PCM [5].

The lower element was in contact with a heat sink with an effective heat transfer coefficient of 600 W/m²K located in ambient of 93 °C. Figure 4 shows the geometry of this system and the boundary conditions. This figure shows the profile of the heat capacity after 5 seconds. The melting front is moving towards the heat sink absorbing and liquefying as the heat is being generated on the top aluminum plate.

This figure also shows that all of the melting capability of the PCM has not been used and the melting front is very close to the electronics. In fact one might try to optimize the system by reducing the size of the PCM and using PCM with lower melting points.

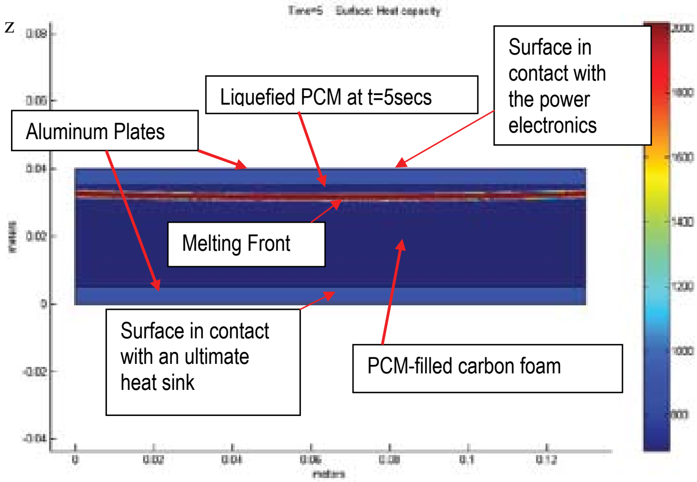

Figure 4. The Geometry of the Graphite System with Melting Front [5].

Figure 5 shows temperature distribution as a function of time for 4 different heights. The z=0.01 m shows the heat sink side and the z=0.04 m shows the electronic side. This figure shows the effect of the PCM after 2 seconds. The temperature gradient of the electronics steadily increases without the PCM, but the PCM has caused the gradient to reduce after 2 seconds.

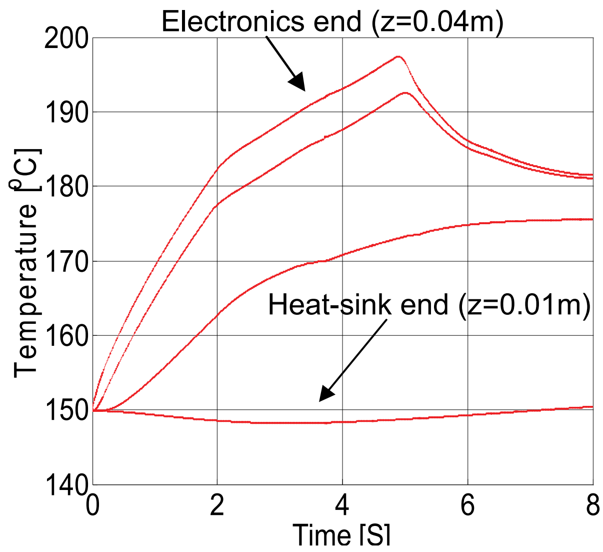

Figure 5. Temperature Distribution Between the Aluminum Plates of the Carbon Fiber Filled PCM as a Function of Time [5].

In all techniques, care should be taken to provide an accurate model of the PCM equivalent heat capacity which is available for that specific PCM. Using CFD packages is a useful and effective way of analyzing PCM so long as the physics of the problems, material properties and boundary conditions are stated properly. Different CFD packages have been used with different techniques. Instead of spending a lot of time setting up the experiment, the CFD packages can quickly shed light into the response of the system, do the what-if scenarios with different PCMs and save valuable time.

References:

1. Shanmugasundaram, V, Brown, J., Yerkes, L., “Thermal management if high heat –flux sources using phase change materials: A design optimization procedure”, American Institute of Aeronautics and Astronautics, 1997
2. Leland, J, Recktenwald, G., “Optimization of a phase change heat sink for extreme environment”, Semitherm, 2003
3. Wirtz, R., Zheng, N., and Chandra, D. “ Thermal management using “Dry” phase change materials”, proceedings of the 1999 Semiconductor Thermal Measurement and Management Symposium (SEMI-THRM), San Diego, California, March 9-11, pp. 74-82, 1999
4. Gauche, P., Weiran, X., “Modeling phase change material in electronics using CFD- A case study”, 2000 International Conference on High-density Interconnect and Systems Packaging, pp 402-407
5. Espinoza, P., Duston, C. “Carbon filled with phase change materials for passive temperature management”, Excerpts from the Proceedings of the COMSOL Multiphysics User’s conference 2005, Boston
6. Alawadhi, E., Amon, C. “PCM thermal control unit for portable electronic devices: Experimental and numerical studies”, IEEE Transactions on Components and Packaging Technologies, 26, 116-125 (2003)

ATS HEAT SINK DISTRIBUTION PARTNERS

DIGI-KEY CORPORATION

- 380+ High Performance Heat Sinks
- Online Ordering
- Next Day Delivery
- Volume Discounts
- Exclusive maxiFLOW™ Technology

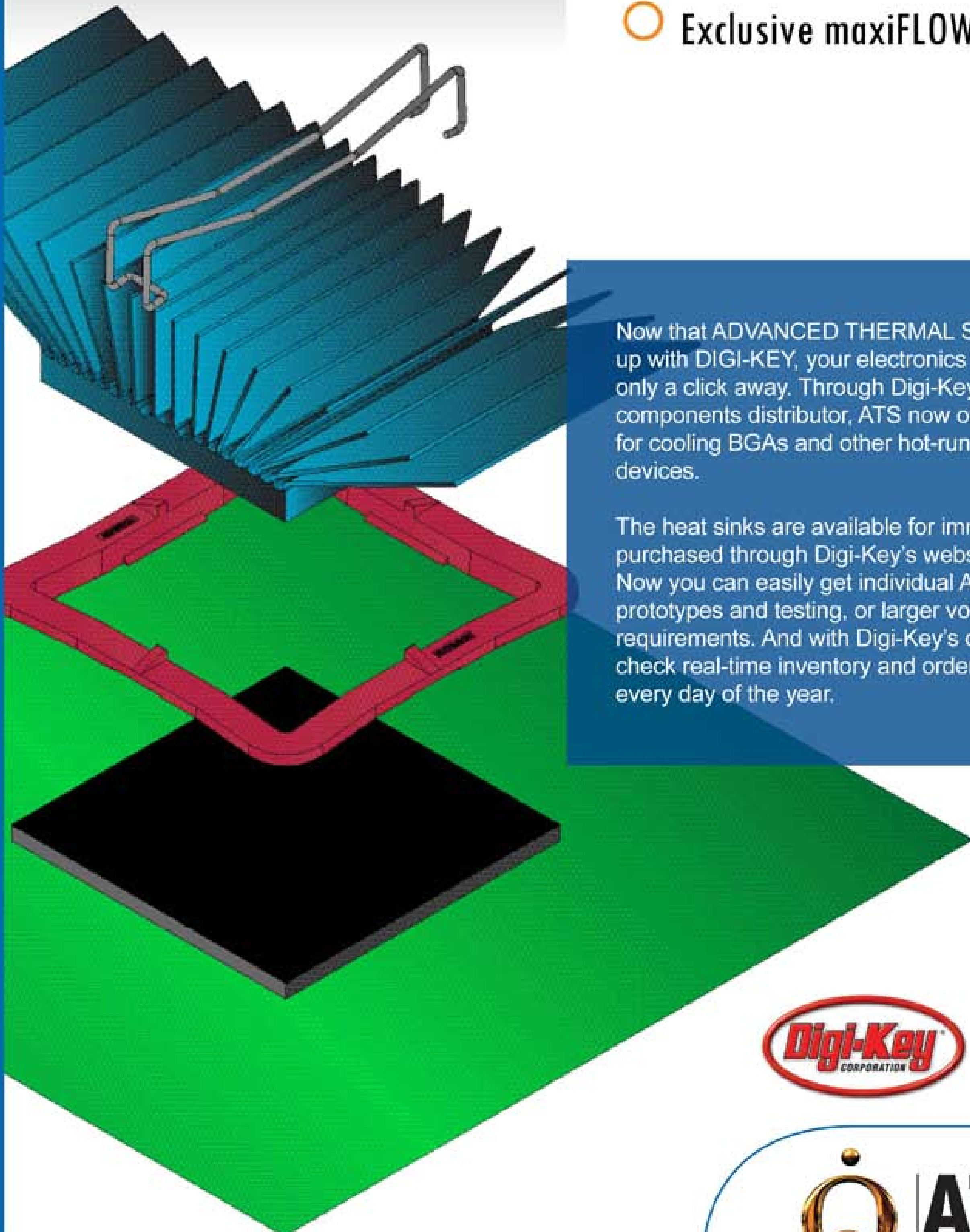

Now that ADVANCED THERMAL SOLUTIONS has teamed up with DIGI-KEY, your electronics cooling solutions are only a click away. Through Digi-Key, the global electronics components distributor, ATS now offers over 380 heat sinks for cooling BGAs and other hot-running semiconductor devices.

The heat sinks are available for immediate delivery when purchased through Digi-Key's website and printed catalogs. Now you can easily get individual ATS heat sinks for prototypes and testing, or larger volumes for production requirements. And with Digi-Key's online tools, you can check real-time inventory and order parts 24 hours a day, every day of the year.

To place an order, please visit www.digikey.com. To download a catalog of ATS heat sinks available through Digi-Key, please visit www.qats.com.

ATS ADVANCED THERMAL SOLUTIONS, INC.
Innovations in Thermal Management®

www.qats.com | 781.769.2800 | 89-27 Access Road Norwood, MA 02062 U.S.A.

COOLING NEWS

Product, Service and Event News from around the Industry

New Honeywell Material Improves Performance of LED Lighting for Displays and Other Applications

Honeywell has developed a new thermal management material that improves energy efficiency of light emitting diodes (LEDs), which are increasingly being used in applications such as street lamps, automotive lighting, flat panel TV displays and computer monitors.

The new product, called Honeywell LTM6300-SP, is a thermal interface material that highly effectively transfers heat generated by LED lamps. As LEDs become smaller, faster and more powerful, more heat is being generated in a confined space, which can threaten to damage the LEDs' performance. If LEDs overheat, they become dim, their color is muted and their lifespans are shortened.

Because LEDs are semiconductor devices, they require more precise heat management than traditional light sources. Honeywell's thermal management materials are designed to meet this specific challenge, helping to effectively transfer heat in semiconductor applications.

LTM6300-SP was designed for LED backlights for flat panel displays, but the packaging technology can be also implemented in LEDs used in a wide range of industries, from automobiles to computers. Honeywell LTM6300-SP is a high-thermal-performance phase change material that is superior to silicone-based products, which typically pump out and degrade at high temperatures.

The lighting industry has evolved from incandescent bulbs toward more energy-efficient options such as fluorescent bulbs and LEDs. Demand for LEDs is growing because they have several benefits over traditional light sources, such as lower energy consumption, longer lifespan, and smaller size. They also produce more light per watt than incandescent bulbs, are more durable and faster, and are mercury-free. When used instead of traditional light sources, LEDs also reduce pollution and carbon footprint because they demand less power, which translates into energy savings that result in lower carbon dioxide and mercury emissions.

The phase change material is based on Honeywell's packaging expertise in thermal management. Honeywell LTM6300-SP is designed to be used mainly as a screen printable paste and complements Honeywell's other thermal interface products.

Tripp Lite Introduces Wide 42U Rack Enclosure; Wide Rack Enclosure Helps Keep Mission-Critical Equipment Cool

Tripp Lite has added a new wide 42U model to its popular line of Smart-Rack™ Enclosures. The SR42UBWD enclosure is ideal for high-density installations where cooling efficiency is a key consideration. Its extra width enables cables and PDUs to be mounted to the sides, where they will not block airflow through the enclosure. This as-

sures maximum cooling efficiency for mission-critical rack equipment.

Tripp Lite's new wide 42U SmartRack Enclosure features a 29.5-in. (750mm) width which optimizes airflow through the enclosure; 4 interior vertical posts with unthreaded square hole openings; a 3,000-lb. stationary/2,250-lb. rolling load capacity; and locking, removable and reversible front and rear doors.

For more information on Tripp Lite's new wide 42U SmartRack Enclosure, go to: http://www.tripplite.com/Wide-Enclosure

New Book Expert Focuses on EMI Solutions in EMC Design

A new book, "Advanced Materials and Design for Electromagnetic Interference Shielding," by Dr. Xingcun Colin Tong, PhD, a resercher with Laird Technologies, Inc., focuses on the role that EMI shielding plays in EMC (Electromagnetic Compliance) design and reviews EMI shielding with emphasis on materials and designs across many industry applications.

Features of the book include EMC definitions and requirements, EMI fundamentals and effective methods to overcome challenges, as well as future EMI trends. EMI products are also addressed, including materials, metal-formed gaskets, and connectors.

According to Dr. Tong, Laird Technologies' EMI materials engineer and subject matter expert, the book explores important EMI topics such as shielding materials and design solutions.

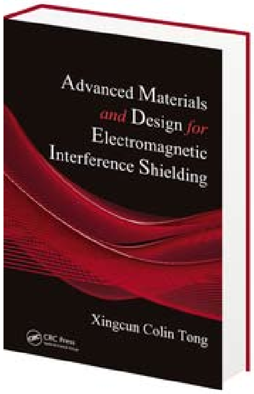

"The purpose of this book is to provide a valuable guide to design engineers that addresses EMI challenges in general, with a focus on shielding materials and design solutions in particular."

Dr. Tong joined Laird technologies in 2006 and has over 20 years' experience in research and development (R&D), property analysis and performance characterization, thermal management of electronic packaging, as well as product manufacturing and component design of advanced materials including EMI shields and metallurgical products. He holds a PhD and Masters of Engineering in Materials Science, as well as a BE in Mechanical Engineering. Based on his R&D activities and industrial practices, Dr. Tong holds several patents and has written more than 30 papers in addition to his new book. He is a member of The Minerals, Metals & Materials Society, IEEE, and ASM International. In addition, Dr. Tong received the Henry Marion Howe Medal from ASM International in 1999 for his contribution to research and development of advanced composite materials.

New Device for Testing and Characterizing Cooling Fans

ATS has introduced the FCM-100 Fan Characterization Module, a specialized unit designed to test and characterize fans of various sizes and performance outputs. Using the FCM-100 Module in conjunction with pressure measurement equipment (such as the PTM-1000) and velocity measurement equipment (such as the eATVS); it is possible to develop fan curves (ΔP vs. Flow rate) that can be used to verify fan manufacturer data

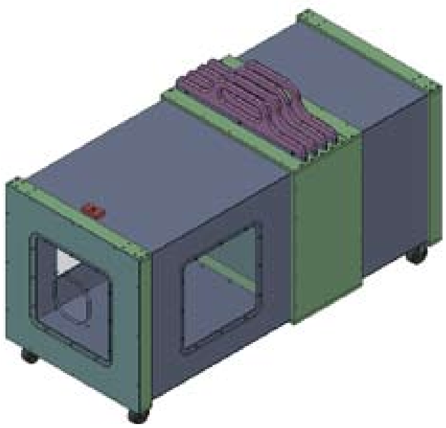

or to characterize fans of unknown performance.

The FCM-100 is constructed of sturdy corrosion resistant sheet metal, with casters for easy portability. A removable and customizable lexan mounting plate is provided to which fans of various diameters can be secured. Four (4) removable perforated flow restriction plates are also provided to allow the user to control the pressure drop through the module for fans under test.

For more information, please contact Advanced Thermal Solutions, Inc. at 781-769-2800 or www.qats.com.